Appl. Phys. A (2016) 122:697
DOI 10.1007/s00339-016-0229-y

Applied Physics A
Materials Science & Processing

Three-dimensional nanostructures of multiwalled carbon nanotubes/graphene oxide/TiO_2 nanotubes for supercapacitor applications

Masoud Faraji[1]

Received: 20 April 2016 / Accepted: 20 June 2016 / Published online: 25 June 2016

Abstract R(fMWCNT-GO)/TiO_2NTs/Ti electrodes with three-dimensional nanostructures were prepared by co-electrochemical reduction of functionalized multiwalled carbon nanotubes (fMWCNTs) and graphene oxide (GO) onto TiO_2 nanotubes/Ti. SEM studies revealed that the reduced fMWCNT-GO hybrid with highly network structures has been uniformly deposited onto the TiO_2NTs arrays. The storage energy performance was investigated by cyclic voltammetry, galvanostatic charge/discharge and electrochemical impedance spectroscopy techniques in 1.0 M H_2SO_4 aqueous solution. The R(fMWCNT-GO)/TiO_2NTs/Ti electrodes exhibit a high specific capacitance up to 600 F g^{-1} at 12 A g^{-1} in 1 M H_2SO_4 and a long cyclic durability with 90 % capacitance retention over 500 cycling, indicating a potential application in electrode material of supercapacitors. The high capacitance of R(GO-fMWCNT)/TiO_2NTs electrode could be attributed to the functional groups of GO-fMWCNT, the 3D structures of the electrode and the highly electrical conductivity fMWCNT.

1 Introduction

Supercapacitors have been considered to be one kind of promising energy storage devices, due to their high power density, fast charge/discharge processes, long cycle life time and rate capability [1]. Based on the energy storage mechanisms, supercapacitors can be classified into two categories, electrical double-layer capacitors (EDLCs) and pseudocapacitors (redox supercapacitors) [2]. In the former, energy storage arises mainly from the ion absorption/desorption process at the interface of the electrode material and the electrolyte. Therefore, enlarging the specific surface area of an electrode is a key factor in obtaining high specific capacitance [3]. In the latter, fast Faradaic reactions take place at the electrode materials [4]. A pseudocapacitor typically exhibits higher capacitance than an EDLC, while the cyclability is not as high as in EDLC [5]. Therefore, a combination of EDLC and pseudocapacitance is preferred. Graphene oxide (GO) or reduced graphene oxide (RGO) used as an EDLC has recently attracted tremendous interest because of their unique thermal, mechanical and electrical properties [2, 6]. However, GO/RGO sheets tend to restack together due to strong van der Waals interaction in the fabrication process of electrodes for supercapacitor applications [2, 7]. As a result, the surface area of GO/RGO cannot be fully utilized, and the specific capacitance might thus be largely decreased. As recently demonstrated, the stacking of GO/RGO sheets can be effectively inhibited by introducing one-dimensional CNTs to form 3D hierarchical structure film where the electrolyte-accessible surface area of GO/RGO is enhanced [8]. This unique mesoporous network can provide conducting pathway to facilitate a fast electrochemical kinetic process during high current density charge/discharge [8, 9]. In addition, CNTs can also efficiently improve the overall electrical and mechanical properties of the hybrid film [10]. Generally, the fabrication of the electrodes based on the GO/RGO-CNT hybrid for supercapacitor applications can be performed via the physical mixing of GO-CNT composites and a polymer binder in a solvent and then coating or dropping of the resulting mixture on a substrate

✉ Masoud Faraji
ma.faraji@urmia.ac.ir

[1] Electrochemistry Research Laboratory, Department of Physical Chemistry, Chemistry Faculty, Urmia University, Urmia, Iran

[2, 9–12]. Therefore, the thickness and amount of the film deposited on substrate can not be better controlled and results the decrease of specific capacitance, cycle life and conductivity of the electrode might be expected. Moreover, the binder may block some pores that can act as ion diffusion path, being not favorable for solution ion to diffuse within inner space of electrode [8]. Despite this fact, it seems that the electrodes based on the RGO/GO-CNT composite still possess high potential for further investigation for supercapacitor applications especially if fabrication procedure of the electrodes containing binder-free RGO/GO-CNT hybrid and the microstructure properties of substrate for deposition of the composite could also be improved. The mesoporous properties of a substrate can significantly affect the deposition and microstructures of active materials leading to high charge/discharge capacities and short diffusion paths for ion transport that are expected to improve the performance of electrochemical supercapacitors [13, 14].

In the present work a new and simple strategy to produce binder-free GO-MWCNT hybrids modified electrodes for supercapacitor applications has been presented. Herein, the modified electrodes were prepared by simple co-electrochemical reduction of functionalized multiwalled carbon nanotubes (fMWCNTs) and graphene oxide (GO) onto the previously formed TiO_2 nanotubes. To the best of our knowledge, this work is the first report about co-electrochemical reduction of fMWCNT and GO on the substrate for supercapacitor applications. The especial ordered structure of TiO_2 nanotubes fabricated by anodizing titanium seems to increase the dispersion of GO-MWCNT and result in the enhancement of capacitance.

2 Experimental procedure

2.1 Preparation of the R(fMWCNT-GO)/TiO_2NTs/Ti electrode

Highly oriented titanium dioxide nanotube arrays (TiO_2-NTs) were prepared via potentiostatic anodization of Ti metal sheet (99 % purity) with a geometric area of 3 cm^2 in a two-electrode electrochemical cell. Very briefly, Ti sheets were polished with emery paper nos. 400–3000 to obtain a mirror finish and subsequently cleaned in acetone and deionized water in an ultrasonic bath. These cleaned titanium sheets were anodized at 30 V for 2 h in ethylene glycol containing 0.5 wt% ammonium fluoride and 2.5 wt% of water at room temperature using a two-electrode system with a platinum foil with a geometric area of 9 cm^2 as cathode where the distance between the two electrodes was 2 cm. The anodized samples were further soaked and washed with deionized water and ultrasonically cleaned for 60 s in deionized water to remove surface debris and subsequently dried in air. Annealing treatment at 450 °C for 2 h was followed for a full crystallization of the anodized samples from amorphous phase to anatase phase. GO was synthesized from graphite powder by the Hummers' method [15]. Functionalization of MWCNTs was carried out in a mixture of sulfuric and nitric acid (50 ml, 3: 1v/v) under reflux condition. Prior to the process, purified MWCNTs were sonicated in the acid solution for 2 h to open agglomeration of nanotubes and anchoring acid solution uniformly on the carbon surface. Thereafter, homogenized carbon solution was oxidized under reflux condition at 100 °C for 6 h to introduce functional groups. Fivefold dilution was then applied to the carbon solution to stop oxidation reaction. Stirring and decantation were consecutively conducted for five times and lastly washed with DI water by filtration until the pH of the resultant solution was approximately at 5. The obtained precipitates were finally dried in a vacuum oven at 60 °C and denoted as fMWCNT. GO-fMWCNT dispersed solutions were prepared by adding given amounts of GO and fMWCNT powder to 50 mL of deionized water and sonicated for one hour to enhance exfoliation and separate GO sheets and fMWCNT particles from each other. Co-electrochemical reduction of fMWCNT-GO onto the annealed TiO_2NTs/Ti electrode was carried out galvanostatically at a constant current of −10 mA for the duration of 3000 s in a three-electrode cell using TiO_2NTs substrate as a working electrode, Pt as a counter electrode and Ag/AgCl as a reference where the electrolyte was 1.0 M KNO_3 + 0.3 g l^{-1} exfoliated GO solution + 0.2 g l^{-1} exfoliated fMWCNTs solution. The black-colored, homogeneous and adherent hybrid film was successfully obtained on the TiO_2NTs/Ti substrate and denoted as R(fMWCNT-GO)/TiO_2NTs/Ti electrode. The mass of R(fMWCNT-GO) deposited on the electrodes was about 0.04 mg. Also, the electrochemical reduction of fMWCNT and GO on the TiO_2NTs/Ti substrate was separately carried out at the same conditions to investigate the influence of hybrid on capacitance behavior. These electrodes are denoted as RGO/TiO_2NTs/Ti electrode and RfMWCNT/TiO_2NTs/Ti electrode.

2.2 Characterization and electrochemical studies

Morphological studies were carried out by a scanning electron microscope (Philips, Model XL30). Capacitance measurements were taken by an Autolab PGSTAT302N potentiostat. All electrochemical studies were performed in a conventional three-electrode cell where all potentials are reported against Ag/AgCl reference electrode at room temperature and 1.0 M H_2SO_4 was the electrolyte throughout the studies.

3 Results and discussion

3.1 Morphology characterization

The FT-IR spectra of both MWCNTs and fMWCNTs are shown in Fig. 1. The absorption band at 1600 cm^{-1} is ascribed to the C=C bond of the hexagonal network in MWCNTs. After the oxidation in acidic media, new bands appear. The peaks at 1730, 3400 cm^{-1} and bands from 1380 to 1460 cm^{-1} are attributed to the stretching of C=O bond, O–H and the stretching modes of the C=OH bonds of carboxylic acid, respectively. Hence, the presence of carbonyl and carboxylic acid groups on the surface of fMWCNTs confirms the efficiency of oxidizing process. These functional groups can be efficiently reduced electrochemically at room temperature where no extra chemicals are employed and the thickness and amount of RfMWCNT film can also be best controlled. Moreover, reduced electrochemically fMWNT containing functional groups not only could effectively influence the pseudocapacitive behavior of the final electrode but also increase its hydrophilicity which is directly related to the electric double-layer capacitance [16]. The microstructure and surface morphology of the obtained electrodes were studied by using scanning electron microscopy (SEM). Figure 2a shows the SEM image of bare TiO_2NTs/Ti electrode where each nanotube has its own wall and is separated from each other. The inner diameter of TiO_2NTs is 40–80 nm, and the wall thickness is 10–20 nm. Highly ordered and vertically oriented TiO_2NTs array offers a high surface area which can significantly increase the dispersion of active materials deposited onto it and result in the enhancement of capacitance. Figure 2b shows SEM micrograph of the RGO/TiO_2NTs where two-dimensional RGO sheets are grown onto the TiO_2 nanotubes. Figure 2c shows TiO_2NTs structure coated well with RMWCNTs by using the electrodeposition method. As can be seen from Fig. 2c, RMWCNT particles are very long and they were randomly deposited onto the TiO_2NTs. Figure 2d and e demonstrates the successful formation of the 3D network structure of the fMWCNT-GO hybrid where RGO sheets and RfMWCNT particles deposited on the TiO_2 nanotubes are visible. The RfMWCNTs act as conductive pathways for electron transport which restrain the close stacking of RGO-coated TiO_2 nanotubes, leading to a three-dimensional loose architecture. This type of morphology can enhance the accessibility of the internal area to the electrolyte and promote the transport of reactive species into the electrode, thereby resulting in increase in the available electrochemically active sites which improve the performance of electrochemical supercapacitors [17, 18]. Moreover, the RfMWCNTs in the hybrid enhance an intimate electronic contact between the RGO and TiO_2NTs and can directly help in the reduction of internal resistance of the R(fMWCNT-GO)/TiO_2NTs/Ti.

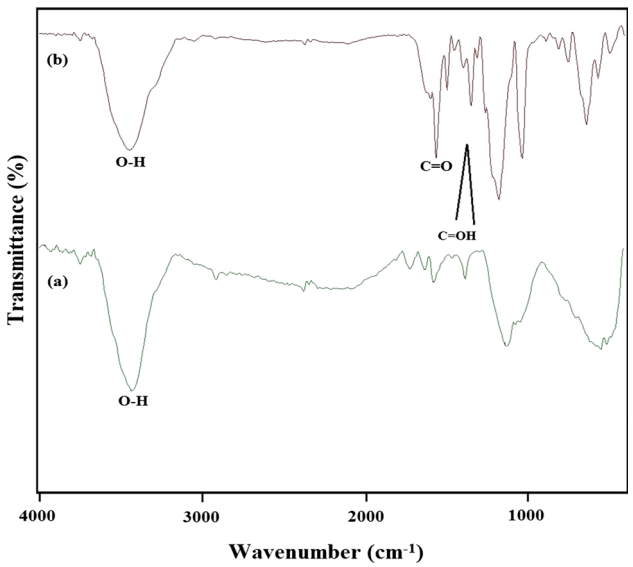

Fig. 1 FT-IR spectra of (*a*) MWCNTs and (*b*) functionalized MWCNTs

3.2 Electrochemical measurements

Figure 3a exhibits the CV curves of the modified electrodes measured at scan rate of 30 mV s^{-1} in 1 M H_2SO_4 solution with the potential range of −0.2–0.6 V versus Ag/AgCl. Pseudocapacitive peaks in CV curves are due to the redox reactions of the RGO and RfMWCNT surface functional groups that take place in acidic media. Such pseudocapacitive peaks of surface functional groups have been previously reported for mesoporous carbon electrodes in acidic electrolytes [11, 19, 20]. It seems that the carbon–oxygen bounds may be involved in the following redox reactions:

$$C* = O + 2e^- + 2H^+ \leftrightarrow C*H - OH$$

$$C - OH \leftrightarrow C = O + H^+ + e^-$$

$$C = O + e^- \leftrightarrow C - O^-$$

The presence of surface functional groups can enhance the capacitance due to the redox reaction of oxygen-based groups and also can improve the wettability of the hybrid surface by the formation of polar functional groups [19]. Although the CV shapes of the three electrodes are similar, peak current for the R(fMWCNT-GO)/TiO_2NTs/Ti electrode is higher. This improvement is due to the higher surface area produced by the three-dimensional structure of this electrode (see Fig. 2d and e) that enhances the accessibility of the interface to ions.

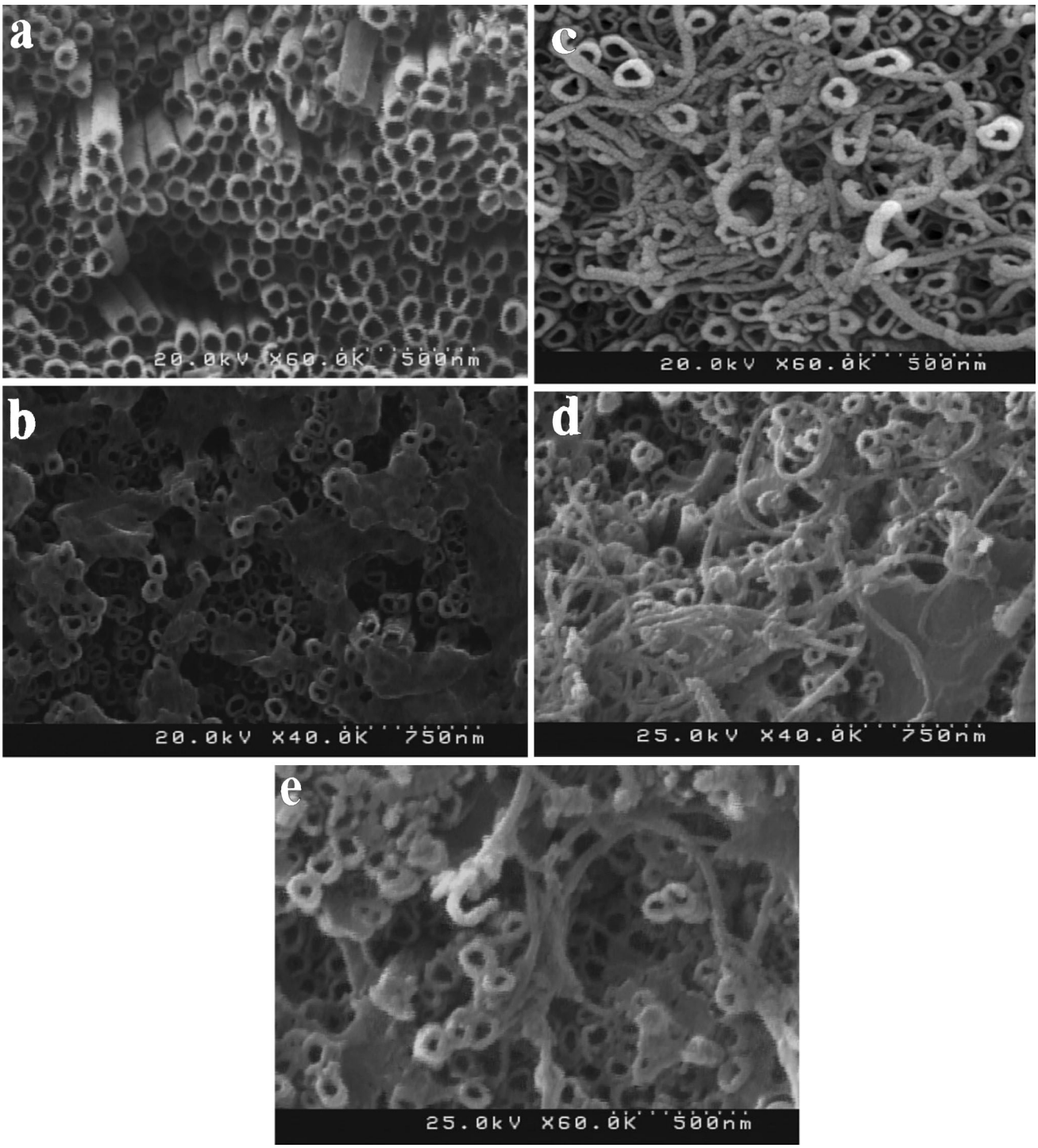

Fig. 2 SEM images of bare TiO_2NTs/Ti electrode (**a**), RGO/TiO_2NTs/Ti electrode (**b**), RfMWCNT/TiO_2NTs/Ti (**c**) and R(fMWCNT-GO)/TiO_2NTs/Ti (**d**, **e**)

The specific capacitance of the modified electrodes was calculated from the CV curves in Fig. 3a, by integrating the area under the current–potential curve:

$$C_{SP} = |q|/_{m.\Delta V} \quad (1)$$

In Eq. (1) m, V, |q| are indicative of the mass of the electroactive materials, the potential window of CV and the average voltammetric charge as integrated from the areas under the positively and negatively swept voltammograms and divided by the sweep rate, respectively [13, 14]:

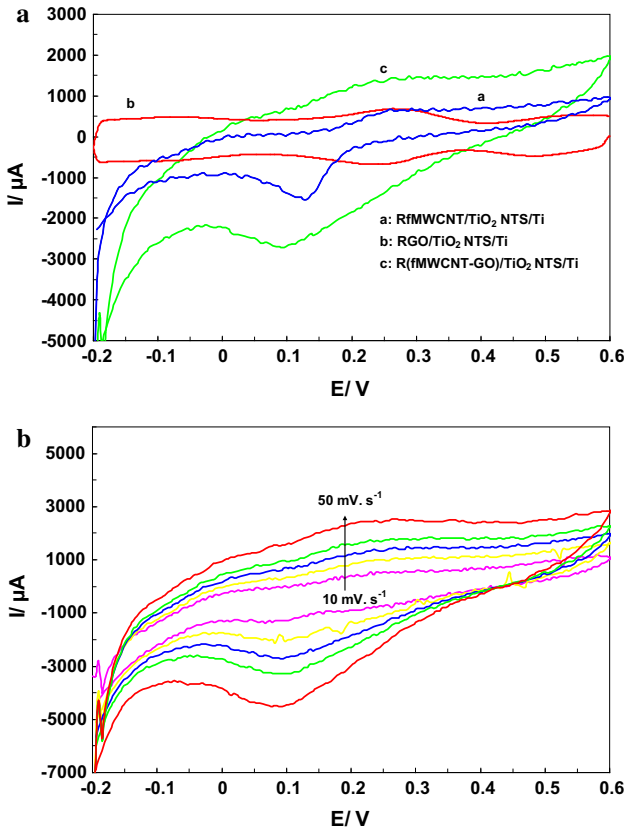

Fig. 3 **a** Cyclic voltammograms of the fabricated electrodes in 1.0 M H_2SO_4 solution at a scan rate of 30 mV s^{-1}. **b** Cyclic voltammogram plots at various scan rates in 1.0 M H_2SO_4 for the R(fMWCNT-GO)/TiO_2NTs/Ti electrode

$$q = \frac{1}{v}\int i\, dV \tag{2}$$

and then averaged according to:

$$|q| = \frac{|q|_{positive\ sweep} + |q|_{negative\ sweep}}{2} \tag{3}$$

Using Eq. (1), the specific capacitance of 530 F g^{-1} is obtained at 30 mV s^{-1} in 1.0 M H_2SO_4 electrolyte for R(fMWCNT-GO)/TiO_2NTs/Ti electrode, compared to 390 F g^{-1} and 280 F g^{-1} for RfMWCNT/TiO_2NTs/Ti and RGO/TiO_2NTs/Ti electrodes, respectively.

The effect of different scan rates on the capacitive behavior of the R(fMWCNT-GO)/TiO_2NTs/Ti electrode has been studied, and results are presented in Fig. 3b. The specific capacitance of the R(fMWCNT-GO)/TiO_2NTs/Ti electrode at different scan rates is high and changes from 540 to 500 F g^{-1}, as the scan rate is increased from 10 to 50 mV s^{-1}. The high specific capacitance obtained at different scan rates can be attributed to the higher surface area produced by the 3D nanostructure of this electrode (see Fig. 2d and e) that enhances the accessibility of the

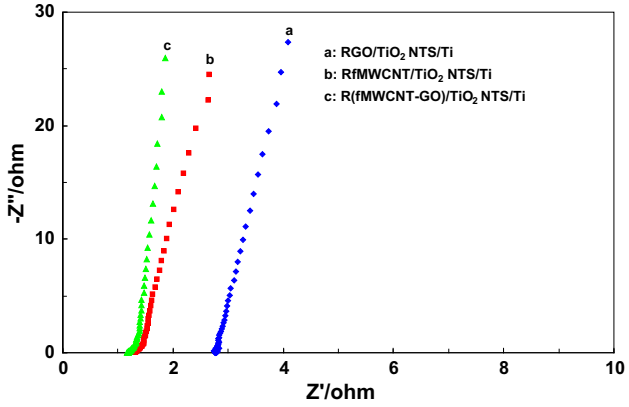

Fig. 4 Impedance Nyquist plots at applied voltage of 0.2 V in 1.0 M H_2SO_4 for the fabricated electrodes

interface to ions. The decreasing capacitance suggests that parts of the surface of the electrode are inaccessible at high charge/discharge rates [21].

Electrochemical impedance spectroscopy (EIS) was carried out to gain insight of the electrochemical behavior of the electrodes such as ion transport behavior and conductivity of the electrodes. The Nyquist plots of obtained electrodes at potential 0.2 V versus Ag/AgCl within the frequency range from 100 kHz to 0.1 Hz in 1.0 M H_2SO_4 are presented in Fig. 4. All the impedance plots are composed of a very small semicircle in the high-frequency region and a straight line with approximate angle of 90° in the low-frequency region. The intersection point of the Nyquist plot with the real impedance axis at high frequency is the measurement of the equivalent series resistance (R_s) of the electrode, while the semicircle diameter corresponds to the charge-transfer resistance (R_{ct}) of the electrodes and electrolyte interface [22]. No distinct semicircle in the plots indicates a very small R_{ct} at the modified electrode/electrolyte interface. The linear segment of the R(fMWCNT-GO)/TiO_2NTs/Ti Nyquist plot is more close to a vertical line along the imaginary axis compared to RfMWCNT/TiO_2NTs/Ti and RGO/TiO_2NTs/Ti electrodes, representing faster kinetics of the diffusion process and the adsorption onto the R(fMWCNT-GO)/TiO_2NTs/Ti electrode surface, suggesting the ideally capacitive behavior of the electrode [22]. As can be seen from Fig. 4, R(fMWCNT-GO)/TiO_2NTs/Ti and RfMWCNT/TiO_2NTs/Ti electrodes possess lower R_s than RGO/TiO_2NTs/Ti electrode, which is due to high conductivity of fMWCNT and increased ion diffusion within the R(fMWCNT-GO)/TiO_2NTs/Ti electrode due to the enhanced compatibility between the electrode and the electrolyte [23]. The improvement of the ohmic resistance directly improves the power density. Since the power density is expressed by $V^2/4R$, where V is the potential difference between two electrodes and R is the

equivalent series resistance, we expect the power density to be improved by a factor of 2 for R(fMWCNT-GO)/TiO_2-NTs/Ti and RfMWCNT/TiO_2NTs/Ti electrodes.

Figure 5a shows the galvanostatic charge/discharge behavior of the electrodes examined in 1.0 M H_2SO_4 electrolyte at a constant current of 12 A g^{-1}. The total gravimetric specific capacitances were calculated from the galvanostatic charge/discharge curves using the following equation [5]:

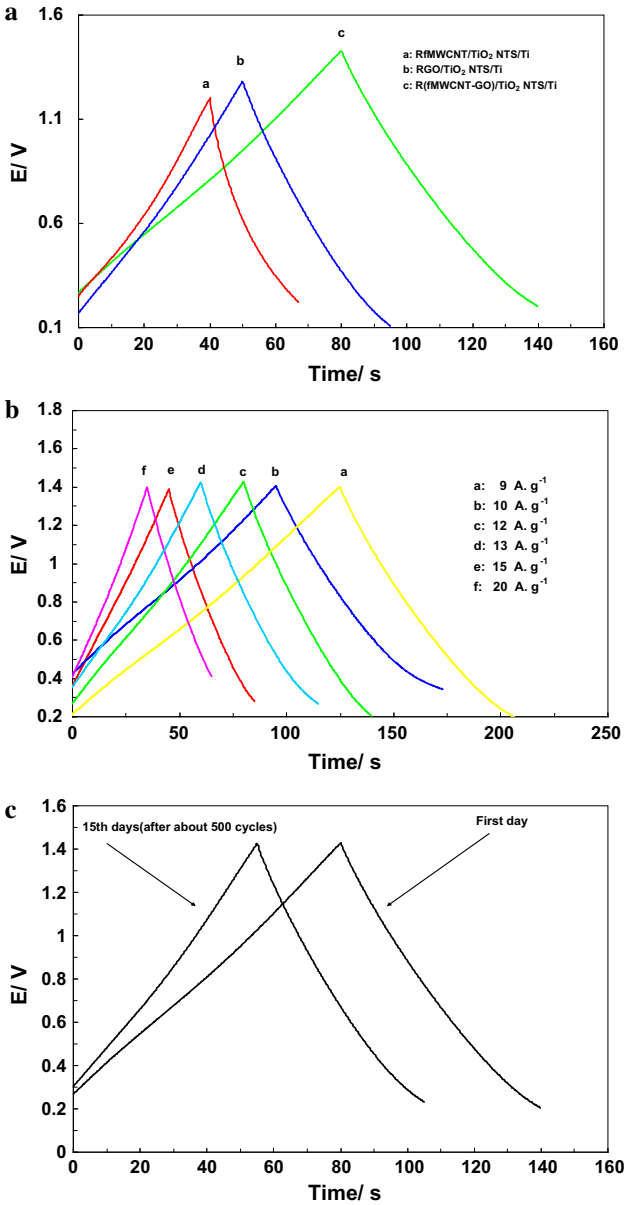

Fig. 5 **a** Galvanostatic charge/discharge curves of the electrodes examined in 1.0 M H_2SO_4 electrolyte at a constant current of 12 A g^{-1}. **b** Galvanostatic charge/discharge cycling curves at different current densities in 1.0 M H_2SO_4 for the R(fMWCNT-GO)/TiO_2NTs/Ti electrode. **c** Charge/discharge curves for the R(fMWCNT-GO)/TiO_2NTs/Ti electrode in 1.0 M H_2SO_4 electrolyte at a current density of 12 A g^{-1} for the first and 15th dyes

$$C_{SP} = (I \times \Delta t)/(\Delta V \times m) \quad (4)$$

where C_{Sp} is the specific capacitance of the electrode (F g^{-1}), I is the charge/discharge current, Δt is the discharge time, ΔV is the potential window, and m is the mass of active material. Using Eq. (4), the specific capacitance of 600 F g^{-1} is obtained at a current density of 12.0A g^{-1} in 1.0 M H_2SO_4 electrolyte for R(fMWCNT-GO)/TiO_2NTs/Ti electrode, compared to 490 and 400 F g^{-1} for RfMWCNT/TiO_2NTs/Ti and RGO/TiO_2NTs/Ti electrodes, respectively. High specific capacitance of the R(fMWCNT-GO)/TiO_2NTs/Ti electrode can be contributed to the abundant porosity of electrode, which favors a high accessible active surface area and easy charge transport mechanism to improve the electron conductivity [24]. As can be seen, the charge/discharge curve of the R(fMWCNT-GO)/TiO_2NTs/Ti electrode is linear and symmetrical with no obvious iR drop, indicating the good capacitive behavior and good electrochemical reversibility of the electrode. The IR drop in the discharge process of the electrode prepared in this work is much smaller compared to those reported in the literature where other methods have been used for the preparation of electrodes based on CNT-GO hybrid in supercapacitor application [2, 9–12, 25–29]. Also, linearity and symmetry of the galvanostatic charge/discharge curve of the modified electrode are superior compared to the mentioned literature. The symmetry of the charge and discharge curve exhibits excellent reversibility forward and backward reaction process [22]. Figure 5b shows the galvanostatic charge/discharge curves of the R(fMWCNT-GO)/TiO_2-NTs/Ti electrode examined in 1.0 M H_2SO_4 electrolyte at different current densities. The maximum specific capacitance for the R(fMWCNT-GO)/TiO_2NTs/Ti reaches 620 F g^{-1} at a current density of 9.0 A g^{-1}, while the specific capacitance remains relatively high (600 F g^{-1}) at a high current density of 20.0 A g^{-1}, implying that the R(fMWCNT-GO)/TiO_2NTs/Ti electrode has a relatively good rate capability at high current densities [5, 24]. Almost, these values are close to that obtained by CV method. In order to evaluate the stability of the R(fMWCNT-GO)/TiO_2NTs/Ti electrode, the specific capacitance in 1.0 M H_2SO_4 electrolyte at a constant current of 12 A g^{-1} was measured in various experiments and numerous cycles of charge/discharge (after about 500 cycles) in a period of 15 days. Figure 5c shows charge/discharge curves of the first cycle and a similar cycle for the sample used in various electrochemical studies for a period of 15 days. A moderate decrease in specific capacitance from 600 to 550 F g^{-1} has been witnessed, showing 90 % perseverance of capacity. The higher cycle performance of the R(fMWCNT-GO)/TiO_2NTs/Ti electrode can be attributed to the mechanical and chemical

stability of binder-free fMWCNT-GO hybrid. The conductive MWCNT network can act as elastic and strong skeleton network for sustaining GO sheets, keeping them away from aggregation and alleviating the irreversible structural damages of GO during cycling.

4 Conclusion

The multiwalled carbon nanotubes graphene oxide hybrid with three-dimensional architectures was successfully synthesized through the co-electrochemical reduction of functionalized multiwalled carbon nanotubes and graphene oxide onto TiO_2 nanotubes fabricated by anodizing of Ti. The resulting binder-free hybrid showed excellent electrochemical performance, especially in electrical conductivity, specific capacitances and cycling stability, offering great potential for application in high-power electrical sources.

Acknowledgments This study was supported by the Office of Vice Chancellor for Research of Urmia University Research Project No. 004/S/94.

References

1. F. Lu, M. Qiu, X. Qi, L. Yang, J. Yin, G. Hao, X. Feng, J. Li, J. Zhong, Appl. Phys. A **104**, 545 (2011)
2. X. Cui, R. Lv, R.U. Rehman, Sagar, C. Liu, Z. Zhang. Electrochim. Acta **169**, 342 (2015)
3. F. Markoulidis, C. Lei, C. Lekakou, Appl. Phys. A **111**, 227 (2013)
4. D. Schopf, M. Es-Souni, Appl. Phys. A **122**, 203 (2016)
5. Y.J. Qiao, C.S. Li, X.J. Chen, C.S. Jiao, Sci. China Tech. Sci. **55**, 913 (2012)
6. A. Wang, X. Zhou, T. Qian, C. Yu, S. Wu, J. Shen, Appl. Phys. A **120**, 693 (2015)
7. D. Ghosh, S. Giri, S. Dhibar, C. Kumar, Das. Electrochim. Acta **147**, 557 (2014)
8. X. Lu, H. Dou, S. Yang, L. Hao, L. Zhang, L. Shen, F. Zhang, X. Zhang, Electrochim. Acta **56**, 9224 (2011)
9. R.B. Rakhi, H.N. Alshareef, J. Power Sources **196**, 8858 (2011)
10. L. Jiang, L. Sheng, C. Long, Z. Fan, Nano Energy **11**, 471 (2015)
11. H.C. Hsu, C.H. Wang, Y.C. Chang, J.H. Hu, B.Y. Yao, C.Y. Lin, J. Phys. Chem. Solids **85**, 62 (2015)
12. X. Dong, G. Xing, M.B. Chan-Park, W. Shi, N. Xiao, J. Wang, Q. Yan, T.C. Sum, W. Huang, P. Chen, Carbon **49**, 5071 (2011)
13. F. Gobal, M. Faraji, Appl. Phys. A **117**, 2087 (2014)
14. G. Rajeshkhanna, E. Umeshbabu, P. Justin, G. Ranga, Rao. Int. J. Hydrogen Energ. **40**, 12303 (2015)
15. S. William, J.R. Hummers, E.O. Richard, J. Am. Chem. Soc. **80**, 1339 (1958)
16. J. Yun, D. Kim, G. Lee, J.S. Ha, Carbon **79**, 156 (2014)
17. M. Ramezani, M. Fathi, F. Mahboubi, Electrochim. Acta **174**, 345 (2015)
18. D.W. Wang, F. Li, H.M. Cheng, J. Power Sources **185**, 1563 (2008)
19. L.Z. Fan, S. Qiao, W. Song, M. Wu, X. He, X. Qu, Electrochim. Acta **105**, 299 (2013)
20. H.A. Andreas, B.E. Conway, Electrochim. Acta **51**, 6510 (2006)
21. T. Tao, L. Zhang, J. Hao, C. Li, New J. Chem. **37**, 1294 (2013)
22. X. Chen, X. Chen, F. Zhang, Z. Yang, S. Huang, J. Power Sources **243**, 555 (2013)
23. Y. Wei, H. Liu, Y. Jin, K. Cai, H. Li, Y. Liu, Z. Kang, Q. Zhang, New J. Chem. **37**, 886 (2013)
24. Y. Liu, J. Zhang, S. Wang, K. Wang, Z. Chen, Q. Xu, New J. Chem. **38**, 4045 (2014)
25. K.S. Kim, S.J. Park, Electrochim. Acta **56**, 1629 (2011)
26. I. Shakir, Electrochim. Acta **129**, 396 (2014)
27. W. Wang, S. Guo, M. Penchev, I. Ruiz, K.N. Bozhilov, D. Yan, M. Ozkan, C.S. Ozkan, Nano Energy **2**, 294 (2013)
28. Y. Zhang, Z. Zhen, Z. Zhang, J. Lao, J. Wei, K. Wang, F. Kang, H. Zhu, Electrochim. Acta **157**, 134 (2015)
29. H. Zanin, E. Saito, H.J. Ceragioli, V. Baranauskas, E.J. Corat, Mater. Res. Bull. **49**, 487 (2014)